Fabrication of superhydrophobic copper metal nanowire surfaces with high thermal conductivity

Ryota Yamamoto[1], Damian Kowalski[2], Ruijie Zhu[1], Keisuke Wada[1], Yuki Sato[1], Sho Kitano[2], Chunyu Zhu[2], Yositaka Aoki[2], and Hiroki Habazaki[2,*]

[1]Graduate School of Chemical Sciences and Engineering, Hokkaido University, Sapporo, Hokkaido 060-8628, Japan

[2]Division of Applied Chemistry, Faculty of Engineering, Hokkaido University, Sapporo, Hokkaido 060-8628, Japan

* Corresponding author: TEL&FAX +81-11-706-6575, e-mail habazaki@eng.hokudai.ac.jp

Highlights

- Copper metal nanowire surface prepared via copper anodizing for forming hydroxide nanowires and subsequent hydrogen reduction
- Post wet organic coating, the copper metal nanowire surface becomes superhydrophobic
- Even condensed water is removed readily from the surface
- Additionally, the metal nanowires exhibit high thermal conductivity

Abstract

Copper is an important practical metal with a high thermal conductivity that is widely used as a heat exchanger material. However, a liquid film often forms on the Cu surface through water vapor condensation, causing a large resistance to heat transfer. To address this issue, a superhydrophobic Cu metal nanowire surface is developed herein via Cu anodizing in a KOH electrolyte to form $Cu(OH)_2$ nanowires, followed by hydrogen reduction at an elevated temperature and the application of a wet organic coating. The hydrogen treatment reduces the hydroxide to the metal while maintaining the nanowire morphology. The superhydrophobic Cu metal nanowire surface exhibits effective removal of water droplets formed through water vapor condensation. Furthermore, the metal nanowire surface exhibits highly improved heat transfer compared with the $Cu(OH)_2$ nanowire surface. Therefore, the combined process of anodizing and hydrogen reduction is a simple approach that forms an effective superhydrophobic Cu surface with high thermal conductivity.

Keywords: Copper, superhydrophobic, anodizing, nanowires, thermal conductivity, water condensation

1. Introduction

Copper is an important practical metal that is widely used in various applications as a heat exchanger material owing to its high thermal conductivity. The efficiency of Cu heat exchangers, such as heat pumps and refrigeration systems, is significantly reduced by water vapor condensation and frost formation. Therefore, Cu surfaces that can avoid the formation of water droplets, condensation of water vapor, and frost formation are required in various applications. Superhydrophobic surfaces are promising materials to be used in such applications because of the efficient removal of water droplets from their surface and the decrease in significant frost formation on their surface [1, 2].

Several studies have fabricated a superhydrophobic surface on Cu [3-21]. Superhydrophobic Cu surfaces have been prepared via micro/nano-surface roughening and by lowering the surface free energy. Chemical etching, a simple and cost-effective process, is often used to develop rough copper surfaces [5, 14, 17]. A sol-gel process is also used to form superhydrophobic surfaces using controlled microstructures on copper [3, 16]. Such surfaces exhibit improved corrosion resistance and high mechanical stability. Anodizing copper is a facile and suitable process for developing nanostructure-controlled surfaces. Superhydrophobic copper(II) oxide (CuO)-nanoneedle-covered Cu surfaces that have a high corrosion resistance or superior antiscaling performance have been prepared through Cu anodizing in KOH or NaOH alkaline electrolytes [7, 8, 20]. Hierarchically micro-/nano-scale rough surfaces are the better-suited morphology for superhydrophobicity and superoleophobicity. These surfaces have previously been prepared on Cu using a combination of different processes, such as mechanical grinding, photolithography, electrodeposition, chemical etching/deposition, and chemical oxidation [9-12, 17, 22]. Of these surface micro-/nano-structuring techniques, Cu anodizing in various electrolytes can produce a range of nanostructured surfaces, including nanofibers [8, 23-27], nanotubes[28], nanopores [29], nanoparticles [24], and nanosheets [24, 30-32]. Furthermore, anodizing is a facile technique used to form surface morphologies conducive to superhydrophobicity. The nanostructured surfaces obtained through Cu anodizing typically contain oxide or hydroxide, which have lower thermal conductivities than Cu. For heat exchanger applications, the nanostructured surface layers should contain Cu with high thermal conductivity rather than copper oxide or hydroxide.

Herein, the superhydrophobic copper nanowire surface is developed via Cu anodizing to form $Cu(OH)_2$ nanowires; then, hydrogen treatment was performed to reduce the copper hydroxide on the nanowires, followed by wet organic coating. The coated nanowire surface exhibits superhydrophobicity with a water contact angle exceeding 160°. The coated nanowire surface exhibits better resistance to condensed water droplets compared with a smooth or

chemically-etched superhydrophobic Cu surface. This study demonstrates improved thermal conductivity of the metal nanowire surface compared with the $Cu(OH)_2$ nanowire surface.

2. Experimental

The Cu substrate used herein was a 0.3-mm-thick, 99.96% pure Cu plate. This Cu substrate was ultrasonically degreased in acetone for 10 min, and then immersed in an 18 wt% HCl aqueous solution for 10 min to remove the thin surface oxide film prior to anodizing. Cu anodizing was conducted at a constant current density of either 3 or 10 mA cm^{-2} in 3 mol dm^{-3} KOH aqueous electrolyte at 20°C for selected periods. A two-electrode electrochemical cell with a platinum (Pt) counter electrode was used during anodizing. A DC power supply (PAS80-9, Kikusui Electronics Corporation, Japan) was used, and the anodizing voltage was recorded using a multimeter (34460A digital multimeter, Agilent Technologies, USA) connected to a personal computer (PC) during the anodizing. After anodizing, the specimens were washed in Milli-Q water. The anodized specimens were reduced at 300°C in an Ar-10% H_2 mixed gas for 1 h, followed by furnace cooling. The temperature was increased at a rate of 10 K min^{-1} to 300°C. Chemical etching of Cu was conducted in a mixed solution containing 3 mol dm^{-3} HCl and 0.5 wt% H_2O_2 at 60°C for 30 min. Post etching, the specimens were washed in Milli-Q water. The anodized specimens were immersed in 5 mmol dm^{-3} stearic acid (SA) in toluene for the wet organic coating. The hydrogen-reduced and chemically etched specimens were immersed in 1 wt.% 1H, 1H, 2H, 2H-perfluorodecanethiol (PFDT) in ethanol for 1 h. The specimens were washed in the respective solvents and dried after being immersed.

The surface and cross-section morphologies of the specimens were observed using a field emission scanning electron microscope (SEM, Sigma-500, Carl Zeiss AG, Germany). The SEM was operated at an accelerating voltage of 1 kV. The cross-sections were prepared through ultramicrotomy (Power Tome X, RMC, UK) using a diamond knife (Micro Star Technologies Inc., USA). Phases of the specimens were identified using an X-ray diffractometer (RINT-2200,

Rigaku, Japan) with Cu Kα radiation. A Raman spectroscope (XploRa, Horiba, Japan) was used to structurally characterize the specimens. The wavelength of the irradiated laser was 532 nm.

The static and dynamic water contact angles on the specimen surface were measured using a contact angle meter (DM-CE1 optical, Kyowa, Japan) with the FAMAS software. The static water contact angles were measured using a 4-μL water droplet, and the dynamic water contact angles were obtained via an extension/contraction method [33]. The contact angles were measured at four different locations of each specimen, and the average and standard deviation were obtained. The durability of the superhydrophobicity was also examined by immersing the specimen in water, which was stirred at 500 rpm, up to 24 h. Water vapor condensation behavior was observed by cooling the specimens on a Peltier cooling plate of 0°C in a constant temperature and humidity chamber of 25°C and 60% relative humidity. The surface was imaged using a digital camera (Tough TG-5, Olympus, Japan). The thermal conductivity of the specimens was qualitatively examined by measuring the freezing time of the water droplets. The specimens were exposed to 350 μL of water and cooled to −15°C on the Peltier plate.

3. Results and Discussion

3.1. Formation of $Cu(OH)_2$ nanowires through anodizing

The $Cu(OH)_2$ nanowires were formed by anodizing a Cu substrate in a KOH electrolyte. The voltage-time responses of the Cu during anodizing at a constant current density of 3 and 10 mA cm^{-2} (Fig. 1) indicated initial steady-state anodizing voltages of 1.2 and 1.35 V, respectively. This was followed by a steep voltage rise to ~2.0 and 2.4 V, respectively. The voltage rise can be associated with the formation of a compact passive film on the Cu substrate beneath the nanowires. The nanowire layer was detached from the substrate at the anodizing time indicated by the arrows in Fig. 1. The detachment can be caused by the oxygen gas generation involved in anodizing.

The formation of $Cu(OH)_2$ nanowires was confirmed through X-ray diffraction (XRD)

measurement and SEM observations. Figure 2a shows the XRD pattern of the Cu anodized at 3 mA cm^{-2} for 900 s. Apart from the reflections of the Cu substrate, all observed reflections are assigned to an orthorhombic $Cu(OH)_2$ phase. The surface SEM observation (Fig. 2b) reveals that the $Cu(OH)_2$ formed during anodizing has a nanowire morphology with a wire diameter of ~200 nm. The highly magnified image (Fig. 2b) indicates that several nanowires were bundled in the nanowire layer. The thickness of the nanowire layer is ~14 μm, as confirmed from the cross-section SEM observation (Fig. 2c).

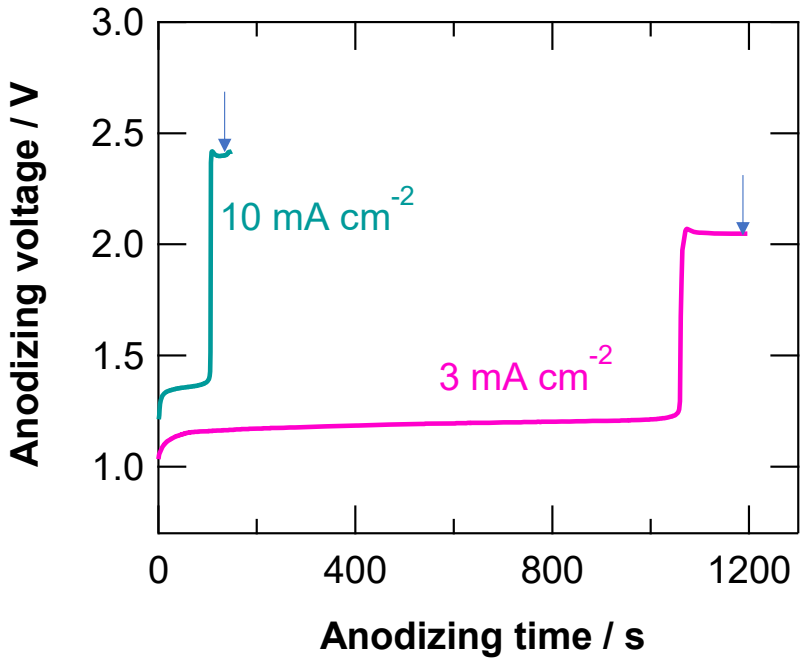

Fig. 1. The voltage-time responses of copper (Cu) during anodizing at a constant current density of 3 and 10 mA cm^{-2} in a 3 mol dm^{-3} KOH electrolyte at 20°C.

The nanowires were further characterized via transmission electron microscopy (TEM, Fig. 2d). The selected area's electron diffraction and high-resolution image indicate that the nanowires are single-crystalline and grow in the <100> direction of the orthorhombic $Cu(OH)_2$ phase. These results are consistent with those of the literature [34]. The Cu^{2+} ions exhibit square planar coordination, and the Cu–Cu chains with bridged hydroxide (OH^-) groups

[35] are oriented to the <100> direction. This becomes the growth direction of the nanowires.

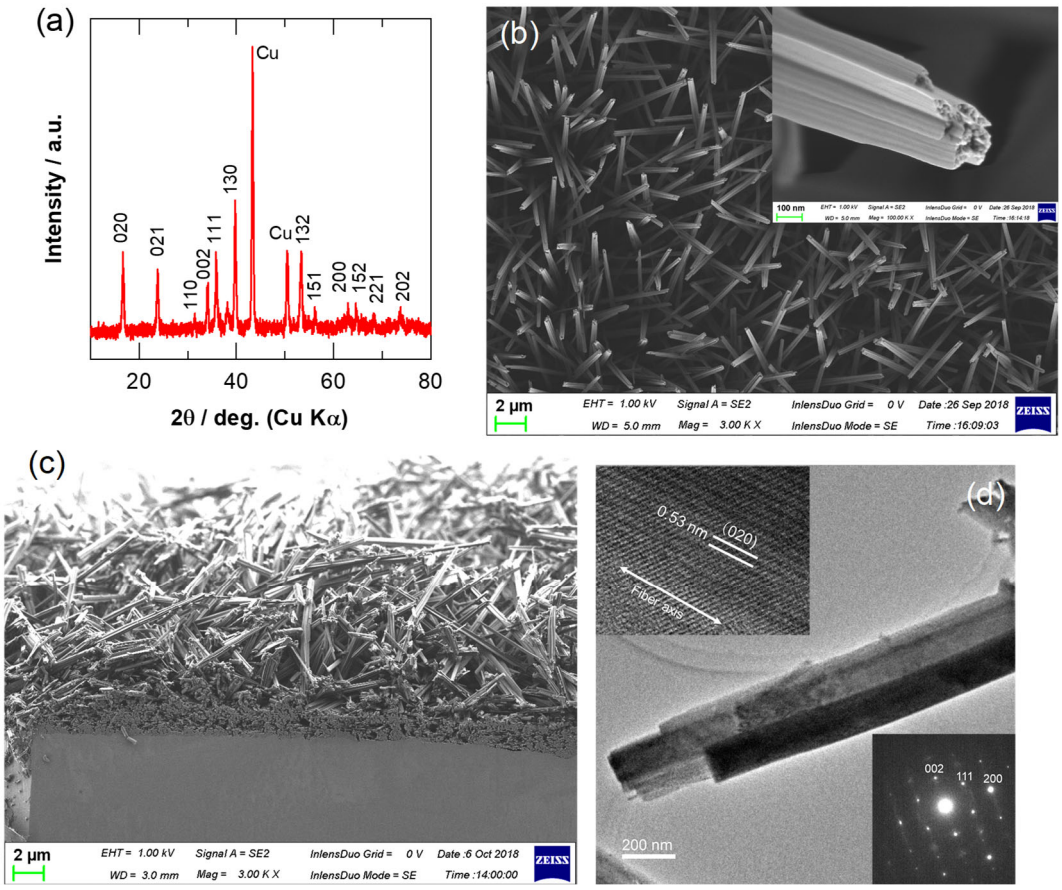

Fig. 2. (a) XRD pattern, (b) surface and (c) cross-section scanning electron micrographs, and (d) transmission electron micrographs with a selected area electron diffraction pattern of Cu anodized at 3 mA cm^{-2} in 3 mol dm^{-3} KOH for 900 s.

In addition, the nanowires were formed when Cu was anodized at a high current density (10 mA cm^{-2}). Figure 3 shows SEM images of the Cu specimens anodized for several periods. Anodizing only for 10 s (Fig. 3a and 3b) develops nanoparticles, not nanowires, and the specimen color changes to dark brown. The formation of nanowires was observed when anodizing was performed for 30 s. The specimen color changes with anodizing time and is associated with the change in the thickness of the $Cu(OH)_2$ nanowire layer. The diameter of the nanowires, at least at the top surface layer, appears to remain almost unchanged with varying anodizing time.

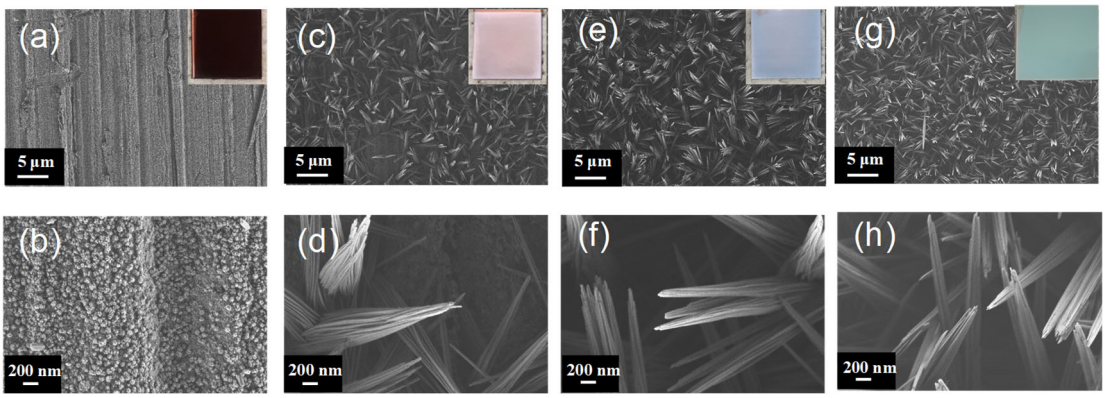

Fig. 3. Scanning electron micrographs of Cu anodized at 10 mA cm^{-2} in 3 mol dm^{-3} KOH electrolyte for (a and b) 10, (c and d) 30, (e and f) 60, and (g and h) 120 s. The inserts show digital camera images of the respective specimens.

The nanoparticles formed by anodizing for 10 s are identified as Cu_2O through Raman spectroscopy (Fig. 4a) [36]. All peaks at 108, 217, and 625 cm^{-1} are assigned as Cu_2O. These peaks are observed in the specimen anodized for 30 s; however, $Cu(OH)_2$ peaks observed at 285, 442, and 487 cm^{-1} also correspond with the formed nanowires. The $Cu(OH)_2$ peaks become stronger after anodizing for 60 s, whereas the intensity of the Cu_2O peaks reduces with anodizing time. The Cu_2O is possibly underneath the $Cu(OH)_2$ nanowires throughout the anodizing time, as illustrated in Fig. 4b.

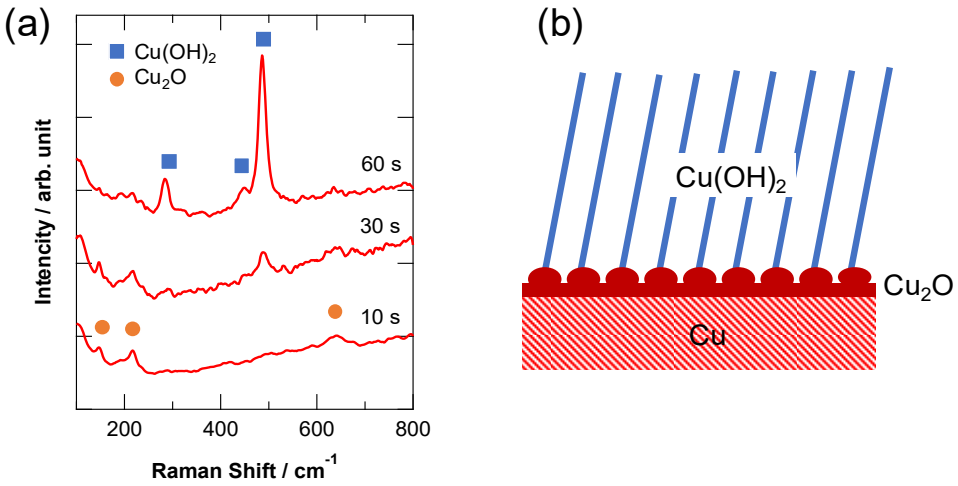

Fig. 4. Raman spectra of copper anodized at 10 mA cm^{-2} in 3 mol dm^{-3} KOH electrolyte for 10–30 s and a schematic showing the cross-sectional morphology of anodized Cu.

3.2. Formation of Cu metal nanowires

When Cu anodized at 10 mA cm^{-2} for 120 s was subjected to hydrogen treatment at 300°C, the specimen color returned to that similar to metallic copper; however, the nanowires maintained the same morphology (Fig. 5a and b). Although each $Cu(OH)_2$ nanowire exhibited a linear shape prior to hydrogen reduction, most nanowires were bent post hydrogen treatment. Such bending can be caused by the stress generated during hydroxide removal. The TEM images of the hydrogen-treated specimen reveal the polycrystalline nature of the metallic Cu phase (Fig. 5c). The metallic Cu phase of the face-centered cubic (fcc) structure is identified from the selected area electron diffraction pattern (the inset of Fig. 5c). The reduction of $Cu(OH)_2$ to metallic Cu was verified using XRD patterns. Figure 6 shows XRD patterns of Cu anodized at 10 mA cm^{-2} for 120 s before and after hydrogen treatment. All $Cu(OH)_2$ peaks completely disappear post hydrogen treatment. The Cu metal nanowires are successfully developed using simple anodizing and subsequent hydrogen treatment. Anodic $Cu(OH)_2$ and Cu_2O nanowires have been reported previously [26, 27, 34, 37]. However, to the best of our knowledge, this is the first successful fabrication of Cu nanowires formed through the reduction of anodic $Cu(OH)_2$ nanowires. This approach is a novel and simple method to fabricate a nanostructured metallic surface layer on common metals, such as iron, nickel, and copper.

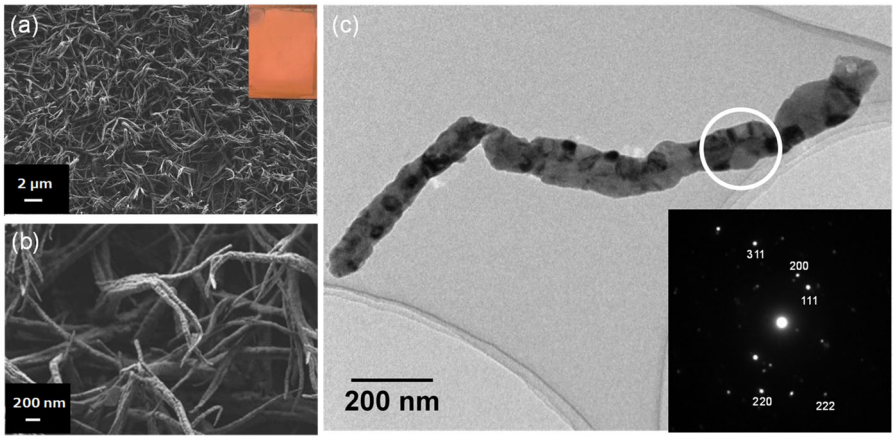

Fig. 5. (a and b) Scanning electron micrographs and (c) transmission electron micrographs of Cu anodized at 10 mA cm^{-2} in 3 mol dm^{-3} KOH electrolyte for 120 s followed by hydrogen treatment at 300°C in the Ar-10% H_2 atmosphere for 3.6 ks. The inset in (c) is the selected area electron diffraction pattern of the circled area.

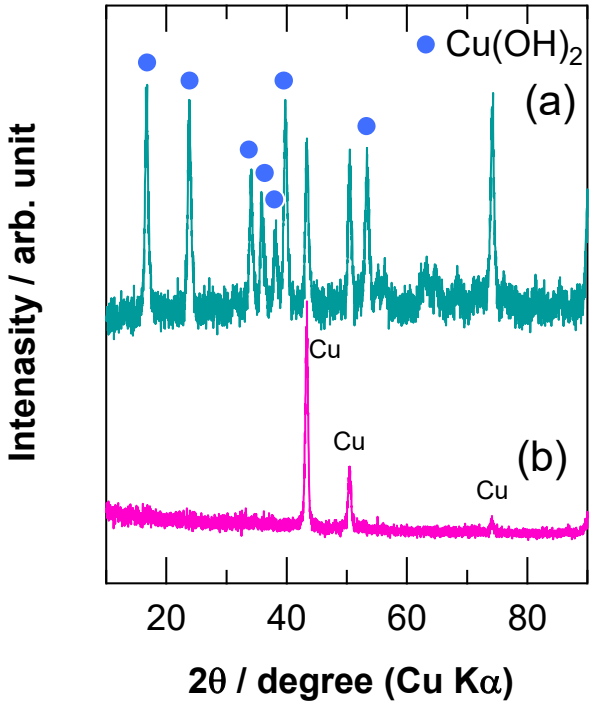

Fig. 6. XRD patterns of Cu anodized at 10 mA cm^{-2} in 3 mol dm^{-3} KOH for 120 s (a) before and (b) after hydrogen treatment at 300°C in the Ar-10% H_2 atmosphere for 3.6 ks.

3.3. Wettability of nanowire surfaces

The wettability of the nanowire surfaces was examined using static water contact angle measurements. Figures 7a and b show the static water contact angles of Cu anodized at 10 mA cm^{-2} for 120 s before and after hydrogen treatment. Both nanowire surfaces exhibit static water contact angles as low as ~2° (superhydrophobic). The water contact angles on rough surfaces are often interpreted using a Wenzel model [38], which correlates the water contact angles on a rough surface (θ_{rough}) to those of the respective flat surface (θ_{flat}), as shown in the following equation:

$$\cos\theta_{\mathrm{rough}} = R\cos\theta_{\mathrm{flat}}, \qquad (1)$$

where R is the roughness factor. Equation (1) suggests that the water contact angle reduces with

increasing roughness when $\theta_{flat} < 90°$ (i.e., on a hydrophilic surface). The solid surface covered with hydroxide, including $Cu(OH)_2$, is known to be hydrophilic. Cu is also always covered with a thin air-formed film, typically comprising oxyhydroxide [39]. The hydrophilic nature, together with a water contact angle of less than 90° of the Cu surface, was reported recently [40]. Both the $Cu(OH)_2$ and Cu nanowires have a high surface area and high roughness factor, contributing to the highly reduced water contact angles close to 0°.

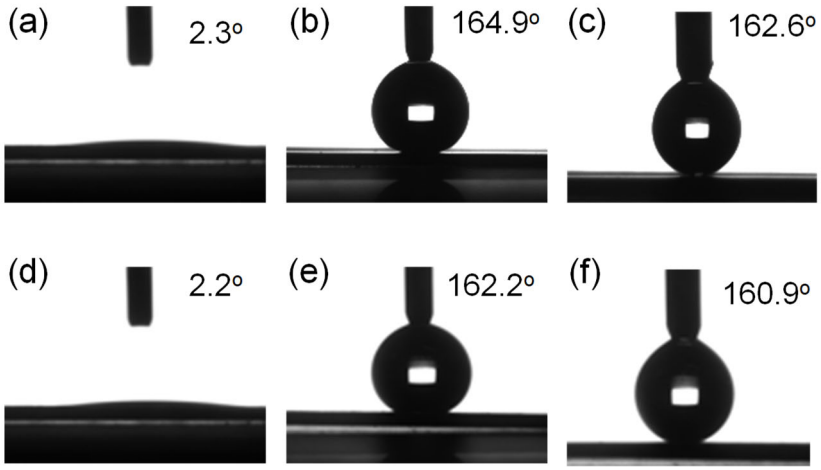

Fig. 7. (a and d) Static water contact angles and (b and e) advancing and (c and f) receding water contact angles of Cu anodized at 10 mA cm^{-2} in 3 mol dm^{-3} KOH for 120 s. (a-c) Before and (d-f) after hydrogen treatment at 300°C in Ar-10% H_2 atmosphere for 3.6 ks. (a, d) Before and (b,c, e, f) after wet organic coating.

Equation (1) also suggests that the water contact angle increases with increasing surface roughness when the surface is hydrophobic ($\theta_{flat} > 90°$). Therefore, the nanowire surfaces were coated with a thin organic monolayer to reduce the surface free energy of the nanowires. Stearic acid coating was selected for the $Cu(OH)_2$ nanowires, whereas PFDT was used to coat the Cu nanowires because alkyl thiols are suitable to form a self-organized monolayer on the Cu surface [41]. Figure 8 shows the XPS spectra of the Cu nanowires before and after PFDT coating. The wide scan XPS spectra (Fig. 8a) discloses the presence of Cu, O and contaminant C elements before the coating. In addition, F peaks, derived from the adsorbed PFDT molecule,

is also detected after the coating. Cu 2p spectra (Fig. 8b) reveals a peak at a binding energy of 932.6 eV for Cu $2p_{3/2}$, corresponding to metallic Cu or Cu(I) species [42]. Before the coating, an additional small Cu $2p_{3/2}$ peak at 934.2 eV is also present together with a broad satellite peak at 938-946 eV, being characteristic of the Cu^{2+} species [42]. Thus, the Cu(II) species were removed during the PFDT coating. In order to distinguish the metallic Cu and Cu(I) species, Cu $L_3M_{4,5}M_{4,5}$ Auger peak region was also measured (Fig. 8c). The peak kinetic energy of 916.6 eV is assigned to Cu(I) species [42]. The metallic Cu peak is also found for the Cu nanowires after the PFDT coating. The presence of Cu(I) species suggests the following formation of fluoroalkylthiol monolayer coating.

$$2RSH + Cu_2O \rightarrow 2RS\text{-}Cu(I) + H_2O \qquad (2)$$

Because of the reaction (2), the surface oxygen peak decreases after the PFDT coating (Fig. 8d). However, the O 1s peak is still remained after the coating, which is similar to the precious study [43]. The intensity of both the lattice O peak at 530.4 eV and the OH-type O peak at 531.7 eV decreases after the coating. The S 2p peak at 162.9 eV (Fig. 8e) F 1s peak at 688.4 eV show the presence of PFDT on the surface of Cu nanowires.

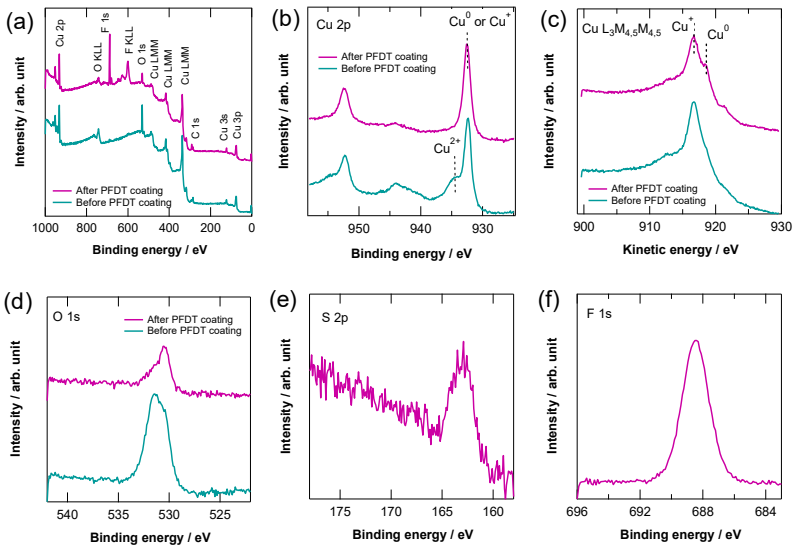

Fig. 8 (a) Wide scan, (b) Cu 2p, (c) Cu $L_3M_{4,5}M_{4,5}$, (d) O 1s, (e) S 2p and (f) F 1s XPS spectra of Cu anodized at 10 mA cm^{-2} in 3 mol dm^{-3} KOH for 120 s, followed by hydrogen treatment at 300°C in Ar-10% H_2 atmosphere for 3.6 ks, before and after the PFDT coating.

The coated $Cu(OH)_2$ nanowires surface reveals the high water contact angles of >150°. The advancing and receding contact angles exceeded 160°. The contact angle hysteresis that is the difference between the advancing and receding contact angles was as low as 2.3°. The low contact angle hysteresis is required for a water droplet to roll off readily from the surface [44]. Therefore, this surface is superhydrophobic (Fig. 7b and c). Similarly, the coated Cu metal nanowire surface is superhydrophobic because the advancing and receding contact angles are 162.2° and 160.9°, respectively. The superhydrophobic Cu nanowire surface was thus successfully fabricated using a simple combination of anodizing, hydrogen treatment, and wet organic coating. Table 1 summarizes the results of the dynamic water contact angles of the $Cu(OH)_2$ and Cu nanowire surfaces obtained via anodizing under the different anodizing conditions. All the coated surfaces shown in Table 1 are superhydrophobic. Anodizing for only 30 s at 10 mA cm^{-2} is sufficient to obtain the superhydrophobic surface.

Table 1 Dynamic water contact angles of Cu anodized at 3 or 10 mA cm^{-2} in 3 mol dm^{-3} KOH electrolyte before and after hydrogen treatment at 300°C in the Ar-10% H_2 atmosphere for 3.6 ks with a wet organic coating.

Nanowire material	**Current density (mA cm^{-2})**	**Anodizing time (s)**	**$\theta_{adv.}$ (°)**	**CAH (°)**
$Cu(OH)_2$	10	30	161.2 ± 0.9	2.8 ± 0.8
	10	60	164.0 ± 1.2	2.5 ± 0.6
	10	120	164.9 ± 1.2	2.3 ± 1.4
	3	900	161.9 ± 1.4	2.4 ± 1.3
Cu metal	10	30	162.8 ± 0.8	1.6 ± 0.6
	10	60	163.3 ± 0.1	2.2 ± 0.3
	10	120	162.2 ± 0.7	1.3 ± 0.5
	3	900	163.3 ± 0.5	1.9 ± 0.6

Effective heat transfer applications of superhydrophobic Cu surfaces require the water vapor condensation behavior to be controlled. Filmwise condensation (formation of the thin liquid film), dropwise condensation (formation of discrete liquid droplets), and jumping droplet condensation (droplet removal via coalescence-induced droplet jumping) are known as water condensation modes. The heat transfer efficiency also increases in this order. The actual condensation behavior of the PFDT-coated Cu nanowire surface was examined herein. The water condensation behavior using a superhydrophobic Cu surface with different surface morphologies was investigated and used as a comparison parameter. Figure 9a shows the scanning electron micrograph of the Cu surface chemically etched in a mixed solution containing 3 mol dm^{-3} HCl and 0.5 wt.% H_2O_2. The chemical etching introduces microscale roughness. The arithmetic mean roughness (R_a) estimated through laser microscopy was 1.38 μm. This rough surface is suitable for achieving superhydrophobicity. The chemically etched Cu surface shows the advancing and receding contact angles and contact angle hysteresis of 164°, 163°, and less than 2° after PFDT coating, respectively (Fig. 9b and 9c).

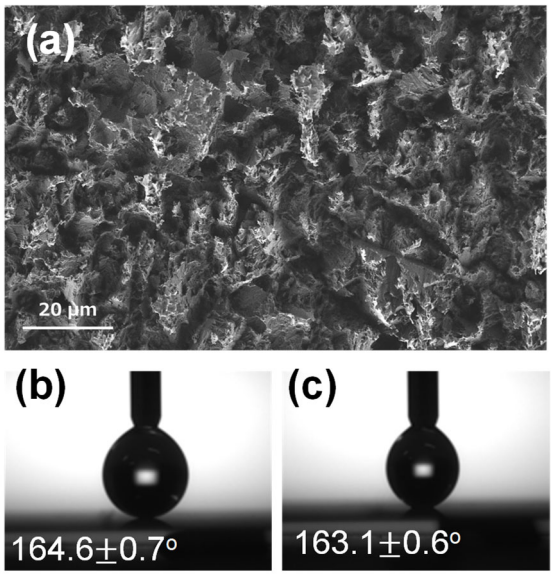

Fig. 9. (a) The scanning electron micrograph of Cu chemically etched in a mixed solution containing 3 mol dm^{-3} HCl and 0.5 wt.% H_2O_2 at 60°C for 1.8 ks and water droplet images on the PFDT coated surface during (b) advancing and (c) receding water contact angles.

The water vapor condensation behavior was examined by cooling the specimen surface on a Peltier cooling stage of 0°C in a chamber that has a constant temperature of 25°C and constant relative humidity of 60%. The PFDT-coated relatively flat Cu surface (Fig. 10a) was hydrophobic with a static water contact angle of 129.5°. The PFDT-coated Cu surface also exhibited dropwise condensation. However, the superhydrophobic Cu nanowire surface (Fig. 10c) exhibited limited water condensation on the surface and is suitable for effective heat transfer. High-speed video recording (Supporting information, Video S1) shows small jumping water droplets on the superhydrophobic Cu nanowire surface. This confirms the jumping droplet condensation mode of this surface. However, the chemically etched superhydrophobic Cu surface (Fig. 10b) shows a higher amount of water condensation than the Cu nanowire surface (Fig. 10c). Furthermore, the entire surface is covered with water droplets despite the surface being superhydrophobic. The size of the water droplets on the chemically etched surface is smaller than that on the flat Cu surface (Fig. 10a), suggesting better heat transfer capability than that of the flat surface.

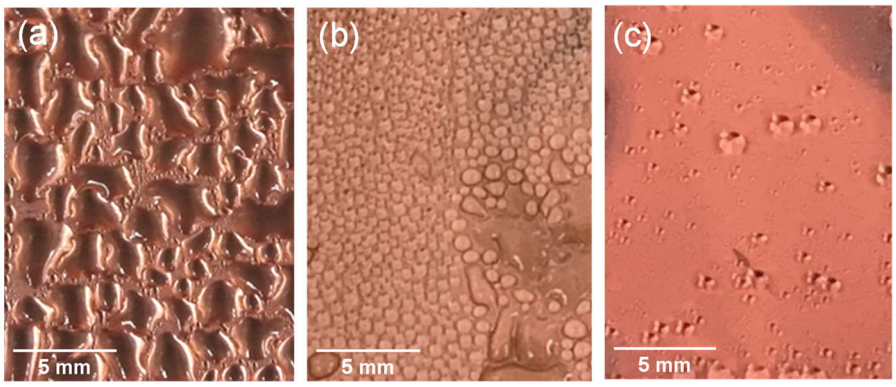

Fig. 10 Digital camera images of (a) as-received Cu, (b) chemically etched Cu, and (c) Cu nanowire surfaces after the water vapor condensation experiment. All surfaces were coated with 1H, 1H, 2H, 2H-perfluorodecanethiol.

Superhydrophobic surfaces have been previously developed by introducing microscale roughness, nanoscale roughness, and micro-/nano-scale hierarchical roughness in addition to

reducing surface free energy [45]. Superhydrophobicity is typically evaluated by measuring static and dynamic contact angles of sessile water droplets and water sliding angles. A Cassie–Baxter state with an air pocket present between the water droplet and rough surface is realized for the sessile water droplets [46]. However, this study demonstrates that the microscale rough surface is in the Wenzel state for condensed water. The Wenzel state shows complete wetting of the rough surface beneath the water droplet for the condensed water droplet, even if the surface is superhydrophobic for a sessile water droplet. The present nanowire morphology is suitable for maintaining a high resistance toward water, even for the condensed water droplets.

The Wenzel state for condensed water on superhydrophobic surfaces with microscale roughness has been reported in the literature [47, 48]. In contrast, high resistance to condensed water droplets has been reported on micro-/nano-hierarchically rough surfaces [49]. Chen et al. reported continuous dropwise condensation on superhydrophobic micropillars covered with short carbon nanotubes [50]. Boreyko et al. experimentally demonstrated the superior dewetting properties of the micro-/nano-dual pillar surface compared with the single micropillar surface [51]. The wetting of the dual pillar surface occurs in two stages: initial wetting of the micropillar roughness followed by nanopillar wetting. The vibration-induced dewetting of a dual pillar surface was also observed after partial wetting. The hierarchical superhydrophobic surfaces do not always show superhydrophobicity for condensed water. The loss of superhydrophobicity during water condensation has been reported for micro-/nano-structured superhydrophobic surfaces [52]. The optimization of the surface morphology and further investigation of the wetting mechanism of the roughened superhydrophobic surfaces using condensed water is necessary to design the necessary surfaces.

This study shows the superior resistance to water of Cu nanowire surfaces with a superhydrophobicity for condensed water. The better-condensed water removal on hydrophobic Cu nanowires has been reported [53], but the surface of the nanowires was prepared using a porous anodic alumina template therein. Therefore, it is not a suitable scalable application. The

fabrication process presented herein for Cu nanowires is simple, scalable, cost-effective, and suitable for real-world applications.

We also examined the durability of the superhydrophobicity by immersing the Cu nanowire specimen in stirring water (Fig. 11). The high advancing contact angle of >160º and the low contact angle hysteresis of <5º remain almost unchanged during the immersion for 24 h. The superhydrophobic Cu nanowires did not show wetting in water during immersion.

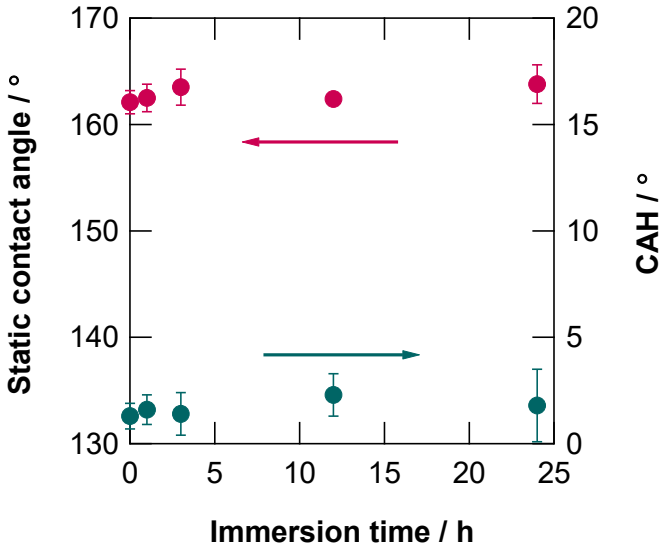

Fig. 11 Change in static contact angle and contact angle hysteresis for water droplet with time of immersion in stirred water.

3.4. Thermal conductivity

The thermal conductivity of the superhydrophobic Cu and $Cu(OH)_2$ nanowire surfaces were qualitatively compared by measuring the freezing time of the water on the cooled superhydrophobic specimens. Figure 12 shows the icing behavior of the superhydrophobic Cu and $Cu(OH)_2$ nanowire specimens, which was cooled at −15°C on a Peltier cooling stage. The result of a flat Cu specimen without coating is also shown for comparison. The icing of the

$Cu(OH)_2$ nanowire specimen occurred ~5 min after reaching the cooling stage of −15°C. The Cu nanowire surface exhibited a shorter icing initiation time of less than 3 min. The Cu nanowire specimen also achieved more icing on the surface compared to the $Cu(OH)_2$ nanowire surface within the same time duration. Both the superhydrophobic surfaces were initially in the Cassie–Baxter state, with the water readily removed by tilting. Therefore, the icing time difference must be associated with the thermal conductivity of the Cu and $Cu(OH)_2$ nanowires. Figure 12 also shows that the icing initiation of the Cu nanowire surface is as fast as that of the flat Cu surface, confirming the high thermal conductivity of the former surface.

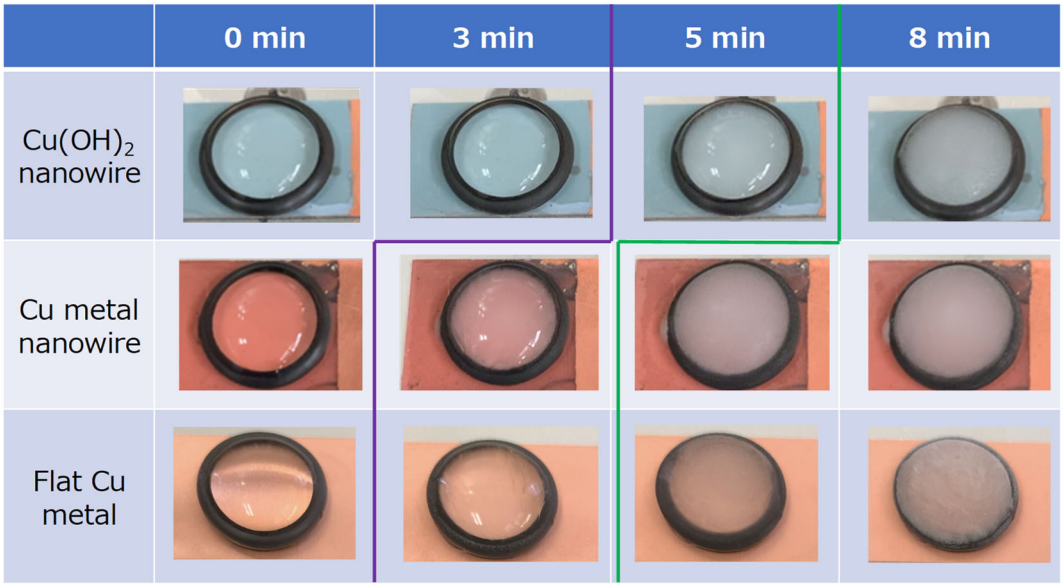

Fig. 12 Digital camera images of Cu anodized at 10 mA cm^{-2} in 3 mol dm^{-3} KOH for 120 s (top) before and (middle) after hydrogen treatment at 300°C in Ar-10% H_2 atmosphere for 3.6 ks as well as non-coated flat Cu metal (bottom) on a Peltier cooling stage of −15°C, monitoring icing behavior of the water. The surfaces were coated with stearic acid and PFDT before and after hydrogen treatment, respectively.

4. Conclusions

Herein, Cu nanowires were prepared through a combination of simple Cu anodizing in a KOH electrolyte and subsequent hydrogen reduction treatment at an elevated temperature. Both nanowire surfaces turned superhydrophobic after being coated with an organic monolayer. Their resistance to water wetting was demonstrated using condensed water on the surface of

the superhydrophobic nanowires. However, the superhydrophobic Cu with microscale roughness became wet by the condensed water. The Cu nanowires exhibited higher thermal conductivity than the $Cu(OH)_2$ nanowires. Thus, this study provides a facile approach for fabricating superhydrophobic Cu surfaces with high thermal conductivity, which are useful in heat exchanger applications.

Acknowledgments

The present study was supported in part by the Hokkaido University Research and Education Center for Robust Agriculture, Forestry and Fisheries Industry. A part of the present study was conducted at the High-Voltage Electron Microscopy Laboratory of Hokkaido University through the "Nanotechnology Platform" Program of the Ministry of Education, Culture, Sports, Science and Technology (MEXT), Japan.

References

[1] K.S. Boyina, A.J. Mahvi, S. Chavan, D. Park, K. Kumar, M. Lira, Y. Yu, A.A. Gunay, X. Wang, N. Miljkovic, Condensation frosting on meter-scale superhydrophobic and superhydrophilic heat exchangers, Int. J. Heat Mass Transfer, 145 (2019) 118694.

[2] N. Miljkovic, E.N. Wang, Condensation heat transfer on superhydrophobic surfaces, MRS Bulletin, 38 (2013) 397-406.

[3] M. Raimondo, F. Veronesi, G. Boveri, G. Guarini, A. Motta, R. Zanoni, Superhydrophobic properties induced by sol-gel routes on copper surfaces, Appl. Surf. Sci., 422 (2017) 1022-1029.

[4] W. Liu, Q.J. Xu, J. Han, X.H. Chen, Y.L. Min, A novel combination approach for the preparation of superhydrophobic surface on copper and the consequent corrosion resistance, Corros. Sci., 110 (2016) 105-113.

[5] W. Liu, Q. Xu, J. Han, X. Chen, Y. Min, A novel combination approach for the preparation of superhydrophobic surface on copper and the consequent corrosion resistance, Corros. Sci., 110 (2016) 105-113.

[6] Z. Khatir, K.J. Kubiak, P.K. Jimack, T.G. Mathia, Dropwise condensation heat transfer process optimisation on superhydrophobic surfaces using a multi-disciplinary approach, Appl. Thermal Eng., 106 (2016) 1337-1344.

[7] F. Xiao, S.J. Yuan, B. Liang, G.Q. Li, S.O. Pehkonen, T.J. Zhang, Superhydrophobic CuO nanoneedle-covered copper surfaces for anticorrosion, J. Mater. Chem. A, 3 (2015) 4374-4388.

[8] W. Jiang, J. He, F. Xiao, S. Yuan, H. Lu, B. Liang, Preparation and Antiscaling Application of Superhydrophobic Anodized CuO Nanowire Surfaces, Industrial & Engineering Chemistry Research, 54 (2015) 6874-6883.

[9] H. Wang, J. Yu, Y. Wu, W. Shao, X. Xu, A facile two-step approach to prepare superhydrophobic surfaces on copper substrates, J. Mater. Chem. A, 2 (2014) 5010-5017.

[10] F.H. Su, K. Yao, Facile Fabrication of Superhydrophobic Surface with Excellent Mechanical Abrasion and Corrosion Resistance on Copper Substrate by a Novel Method, ACS Appl. Mater. Interfaces, 6 (2014) 8762-8770.

[11] J. Ou, W. Hu, S. Liu, M. Xue, F. Wang, W. Li, Superoleophobic textured copper surfaces fabricated by chemical etching/oxidation and surface fluorination, ACS Appl Mater Interfaces, 5 (2013) 10035-10041.

[12] X.T. Zhu, Z.Z. Zhang, X.H. Xu, X.H. Men, J. Yang, X.Y. Zhou, Q.J. Xue, Facile fabrication of a superamphiphobic surface on the copper substrate, J. Colloid Interface Sci., 367 (2012) 443-449.

[13] Z.Z. Zhang, X.T. Zhu, J. Yang, X.H. Xu, X.H. Men, X.Y. Zhou, Facile fabrication of superoleophobic surfaces with enhanced corrosion resistance and easy repairability, Appl. Phys. a, 108 (2012) 601-606.

[14] L. Liu, F. Xu, L. Ma, Facile Fabrication of a Superhydrophobic Cu Surface via a Selective Etching of High-Energy Facets, J. Phys. Chem. C, 116 (2012) 18722-18727.

[15] S. Barthwal, Y.S. Kim, S.H. Lim, Superhydrophobic and superoleophobic copper plate fabrication using alkaline solution assisted surface oxidation methods, I Int. J. Precision Eng. Manufacturing, 13 (2012) 1311-1315.

[16] A.V. Rao, S.S. Latthe, S.A. Mahadik, C. Kappenstein, Mechanically stable and corrosion resistant superhydrophobic sol-gel coatings on copper substrate, Appl. Surf. Sci., 257 (2011) 5772-5776.

[17] Y.F. Zhang, X.Q. Yu, Q.H. Zhou, F. Chen, K.N. Li, Fabrication of superhydrophobic copper surface with ultra-low water roll angle, Appl. Surf. Sci., 256 (2010) 1883-1887.

[18] L. Pan, H. Dong, P. Bi, Facile preparation of superhydrophobic copper surface by HNO3 etching technique with the assistance of CTAB and ultrasonication, Appl. Surf. Sci., 257 (2010) 1707-1711.

[19] Y. Huang, D.K. Sarkar, X.G. Chen, A one-step process to engineer superhydrophobic copper surfaces, Mater. Lett., 64 (2010) 2722-2724.

[20] X.H. Chen, L.H. Kong, D. Dong, G.B. Yang, L.G. Yu, J.M. Chen, P.Y. Zhang, Synthesis and characterization of superhydrophobic functionalized Cu(OH)(2) nanotube arrays on copper foil, Appl. Surf. Sci., 255 (2009) 4015-4019.

[21] Z.G. Guo, F.B. Han, L.B. Wang, W.M. Liu, Fabrication of superhydrophobic copper by wet chemical reaction, Thin Solid Films, 515 (2007) 7190-7194.

[22] X.M. Chen, J.A. Weibel, S.V. Garimella, Exploiting Microscale Roughness on Hierarchical Superhydrophobic Copper Surfaces for Enhanced Dropwise Condensation, Adv. Mater. Interfaces, 2 (2015).

[23] S. Sahoo, S. Husale, B. Colwill, T.M. Lu, S. Nayak, P.M. Ajayan, Electric Field Directed Self-Assembly of Cuprous Oxide Nanostructures for Photon Sensing, ACS Nano, 3 (2009) 3935-3944.

[24] N.K. Allam, C.A. Grimes, Electrochemical fabrication of complex copper oxide nanoarchitectures via copper anodization in aqueous and non-aqueous electrolytes, Mater. Lett., 65 (2011) 1949-1955.

[25] Z. Cheng, M. Du, K. Fu, N. Zhang, K. Sun, pH-controllable water permeation through a nanostructured copper mesh film, ACS Appl Mater Interfaces, 4 (2012) 5826-5832.

[26] P. Kar, M.K. El-Tahlawy, Y. Zhang, M. Yassin, N. Mahdi, R. Kisslinger, U.K. Thakur, A.M. Askar, R. Fedosejevs, K. Shankar, Anodic copper oxide nanowire and nanopore arrays with mixed phase content: synthesis, characterization and optical limiting response, J. Phys. Commun., 1 (2017).

[27] Y. Lv, B. Shi, X. Su, Y. Li, J. Sun, J. Shao, L. Tian, J. Ding, Fabrication and characterisation of Cu_2O nanorods array by anodic oxidation method, Micro & Nano Letters, 13 (2018) 289-291.

[28] L. Xu, Q. Yang, X. Liu, J. Liu, X. Sun, One-dimensional copper oxide nanotube arrays: biosensors for glucose detection, RSC Adv., 4 (2014) 1449-1455.

[29] A.D. Pauric, S.A. Baig, A.N. Pantaleo, Y. Wang, P. Kruse, Sponge-Like Porous Metal Surfaces from Anodization in Very Concentrated Acids, J. Electrochem. Soc., 160 (2012) C12-C18.

[30] J.-F. Xie, Y.-X. Huang, W.-W. Li, X.-N. Song, L. Xiong, H.-Q. Yu, Efficient electrochemical CO2 reduction on a unique chrysanthemum-like Cu nanoflower electrode and direct observation of carbon deposite, Electrochim. Acta, 139 (2014) 137-144.

[31] H. Hu, X. Wang, L. Gong, X. Yu, X. Yang, J. Zhao, Preparation of leaflike copper phosphate films by anodic oxidation and their catalytic oxidation performance, Catal. Commun., 95 (2017) 46-49.

[32] X. Shu, H. Zheng, G. Xu, J. Zhao, L. Cui, J. Cui, Y. Qin, Y. Wang, Y. Zhang, Y. Wu, The anodization synthesis of copper oxide nanosheet arrays and their photoelectrochemical properties, Appl. Surf. Sci., 412 (2017) 505-516.

[33] S. Yang, H. Habazaki, T. Fujii, Y. Aoki, P. Skeldon, G.E. Thompson, Control of morphology and surface wettability of anodic niobium oxide microcones formed in hot phosphate-glycerol electrolytes, Electrochim. Acta, 56 (2011) 7446-7453.

[34] X.F. Wu, H. Bai, J.X. Zhang, F.E. Chen, G.Q. Shi, Copper hydroxide nanoneedle and

nanotube arrays fabricated by anodization of copper, J. Phys. Chem. B, 109 (2005) 22836-22842.

[35] R. Rodriguez-Clemente, C.J. Serna, M. Ocana, E. Matijevic, The relationship of particle morphology and structure of basic copper(II) compounds obtained by homogeneous precipitation, J. Cryst. Growth, 143 (1994) 277-286.

[36] L. Mandal, K.R. Yang, M.R. Motapothula, D. Ren, P. Lobaccaro, A. Patra, M. Sherburne, V.S. Batista, B.S. Yeo, J.W. Ager, J. Martin, T. Venkatesan, Investigating the Role of Copper Oxide in Electrochemical CO_2 Reduction in Real Time, ACS Appl. Mater. Interfaces, 10 (2018) 8574-8584.

[37] H. Hu, X. Wang, L. Gong, X. Yu, X. Xu, J. Zhao, Fabrication of n-Cu_2O films by anodisation and their photoelectrochemical properties, Mater. Lett., 212 (2018) 315-318.

[38] R.N. Wenzel, Resistance of solid surfaces to wetting by water, Ind. Eng. Chem., 28 (1936) 988-994.

[39] S.K. Chawla, B.I. Rickett, N. Sankarraman, J.H. Payer, An X-ray photo-electron spectroscopic investigation of the air-formed film on copper, Corros. Sci., 33 (1992) 1617-1631.

[40] E. Touzé, C. Cougnon, Study of the air-formed oxide layer at the copper surface and its impact on the copper corrosion in an aggressive chloride medium, Electrochim. Acta, 262 (2018) 206-213.

[41] P.E. Laibinis, G.M. Whitesides, Self-assembled monolayers of n-alkanethiolates on copper are barrier films that protect the metal against oxidation by air, J. Am. Chem. Soc., 114 (1992) 9022-9028.

[42] S. Poulston, P.M. Parlett, P. Stone, M. Bowker, Surface oxidation and reduction of CuO and Cu_2O studied using XPS and XAES, Surf. Interface Anal., 24 (1996) 811-820.

[43] G. Fonder, F. Laffineur, J. Delhalle, Z. Mekhalif, Alkanethiol-oxidized copper interface: The critical influence of concentration, J. Colloid Interface Sci., 326 (2008) 333-338.

[44] Y.H. Xiu, L.B. Zhu, D.W. Hess, C.P. Wong, Relationship between work of adhesion and contact angle hysteresis on superhydrophobic surfaces, J. Phys. Chem. C, 112 (2008) 11403-11407.

[45] A.K. Kota, G. Kwon, A. Tuteja, The design and applications of superomniphobic surfaces, NPG Asia Mater, 6 (2014) e109.

[46] A.B.D. Cassie, S. Baxter, Wettability of porous surfaces, Trans. Faraday Soc., 40 (1944) 546-551.

[47] R.D. Narhe, D.A. Beysens, Nucleation and growth on a superhydrophobic grooved surface, Phys. Rev. Lett., 93 (2004) 076103.

[48] K.A. Wier, T.J. McCarthy, Condensation on Ultrahydrophobic Surfaces and Its Effect on Droplet Mobility: Ultrahydrophobic Surfaces Are Not Always Water Repellant, Langmuir, 22 (2006) 2433-2436.

[49] T. Liu, W. Sun, X. Sun, H. Ai, Thermodynamic Analysis of the Effect of the Hierarchical Architecture of a Superhydrophobic Surface on a Condensed Drop State, Langmuir, 26 (2010) 14835-14841.

[50] C.-H. Chen, Q. Cai, C. Tsai, C.-L. Chen, G. Xiong, Y. Yu, Z. Ren, Dropwise condensation on superhydrophobic surfaces with two-tier roughness, Appl. Phys. Lett., 90 (2007).

[51] J.B. Boreyko, C.H. Baker, C.R. Poley, C.H. Chen, Wetting and dewetting transitions on hierarchical superhydrophobic surfaces, Langmuir, 27 (2011) 7502-7509.

[52] H. Jo, K.W. Hwang, D. Kim, M. Kiyofumi, H.S. Park, M.H. Kim, H.S. Ahn, Loss of superhydrophobicity of hydrophobic micro/nano structures during condensation, Sci Rep, 5 (2015) 9901.

[53] R. Wen, Q. Li, J. Wu, G. Wu, W. Wang, Y. Chen, X. Ma, D. Zhao, R. Yang, Hydrophobic copper nanowires for enhancing condensation heat transfer, Nano Energy, 33 (2017) 177-183.

Graphical abstract